Single atom detection from low contrast-to-noise ratio electron microscopy images

Single atom detection from low contrast-to-noise ratio electron microscopy images

J. Fatermans,[1,2] A. J. den Dekker,[2,3] K. Müller-Caspary,[1] I. Lobato,[1] C. O'Leary,[4] P. D. Nellist,[4] and S. Van Aert[1,*]

[1] *Electron Microscopy for Materials Science (EMAT), University of Antwerp, Groenenborgerlaan 171, B-2020 Antwerp, Belgium*

[2] *Imec-Vision Lab, University of Antwerp, Universiteitsplein 1, 2610 Wilrijk, Belgium*

[3] *Delft Center for Systems and Control (DCSC), Delft University of Technology, Mekelweg 2, 2628 CD Delft, The Netherlands*

[4] *Department of Materials, University of Oxford, Parks Road, OX1 3PH Oxford, United Kingdom*

Single atom detection is of key importance to solve a wide range of scientific and technological problems. The strong interaction of electrons with matter makes transmission electron microscopy one of the most promising techniques. In particular, aberration correction using scanning transmission electron microscopy (STEM) has made a significant step forward to detect single atoms. However, to overcome radiation damage, related to the use of high energy electrons, the incoming electron dose should be kept low enough. This results in images exhibiting a low signal-to-noise ratio (SNR) and extremely weak contrast especially for light-element nanomaterials. To overcome this problem, a combination of physics-based model fitting and the use of a model-order selection method is proposed enabling one to detect single atoms with high reliability.

Nanomaterials have attracted increasing scientific interest, because their exact atomic structure may lead to interesting and unexpected physical and chemical properties. Therefore, precise structure determination is crucial to fully understand the structure-properties relation of these materials. Because of several important developments in aberration correction technology [1–3], transmission electron microscopy imaging has become an excellent technique to visualize nanomaterials down to sub-angstrom resolution and thereby solving challenging problems in materials science [4–12].

Precise structure information can be obtained by fitting a physics-based model to the image data. This quantitative model fitting approach is generally referred to as statistical parameter estimation [13–16]. When applied to annular dark-field (ADF) scanning transmission electron microscopy (STEM) projection images of crystalline nanomaterials, an important assumption is that the number of atomic columns is known. For materials that are stable under the electron beam, this number can usually be determined visually from atomic resolution images. For beam-stable materials, the electron dose can indeed be chosen sufficiently large to ensure a high enough signal-to-noise ratio (SNR) and high contrast enabling one to visualize the individual atomic columns. However, for radiation-sensitive and light-element nanomaterials, the incoming electron dose should be kept sufficiently low to avoid radiation damage. As a consequence, the images exhibit a relatively low SNR and, in addition, they show weak contrast [17]. Both aspects cause the images to possess low contrast-to-noise ratio (CNR) values. Local fluctuations of the background or differences in column thickness or composition can cause each atomic column to possess an individual CNR value. The CNR value of the column with the lowest intensity present in an image is referred to as the so-called minimum column CNR of the image. It is defined as the ratio of the total intensity of electrons scattered by the column, the so-called scattering cross-section [16, 18–20], to the square root of the sum of the scattering cross-section and the integrated background under the column. In the absence of a priori knowledge, visual inspection of low CNR images will lead to biased structure information. To overcome this problem, the maximum a posteriori (MAP) probability rule is proposed in this Letter as an alternative, automatic and objective method for single atom detection from low CNR electron microscopy images.

Statistical parameter estimation theory makes use of the fact that the observed image pixel values can be related to physical quantities or parameters. Often, this relationship between the parameters and the pixel values can be described by a mathematical expression or model, which is derived from physical laws. If such first principles based models cannot be derived or are too complex, simplified empirical models may be used. To extract quantitative structure information from atomic resolution STEM images, a superposition of Gaussian functions which are peaked at the atomic column positions has been shown to provide reliable results [16, 18, 21–26]. The model parameters that need to be estimated include a constant background and the peak intensities, widths and coordinates of all atomic columns in the image. This is opposed to other maximum likelihood methods where estimation is performed on the level of single pixels [27, 28].

In order to reliably quantify the number of atomic columns, the MAP probability rule is introduced to select the most probable number of atomic columns and hence the number of Gaussian functions needed. This model-order selection criterion is a direct consequence of Bayes' theorem, which allows one to write the probability of a certain event in terms of conditions that can be related to that event [29, 30]. Interestingly, MAP probability is claimed to be an optimal selection rule in the

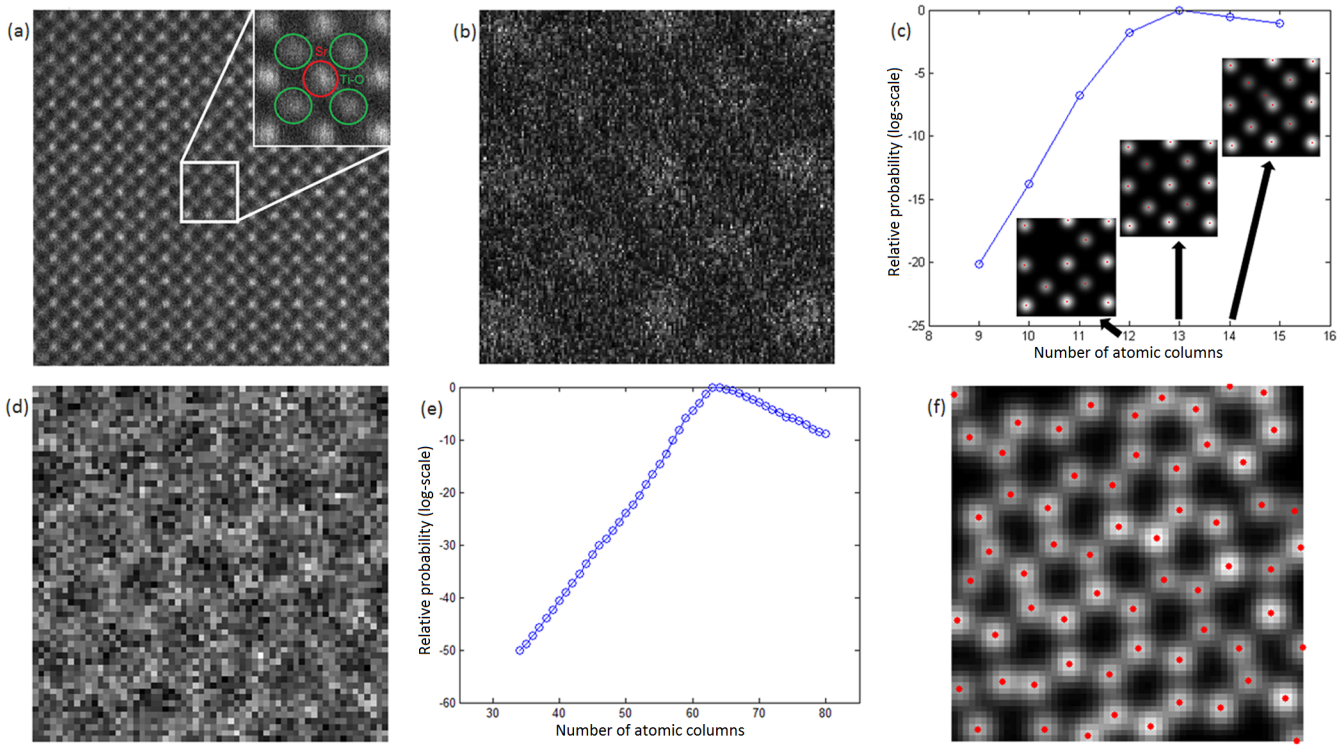

FIG. 1. (a) HAADF image of $SrTiO_3$ [100] with an incoming electron dose of $(9.1 \pm 0.4) \cdot 10^5$ $e^-/Å^2$ and a minimum column CNR of 71.6. The region indicated by the square has been magnified in the inset where Sr columns and Ti-O columns are indicated in red and green, respectively. (b) Noisier counterpart of the inset in (a) with an incoming electron dose of $(1.08 \pm 0.05) \cdot 10^4$ $e^-/Å^2$ and a minimum column CNR of 5.2. (c) MAP probability rule evaluated for the experimental data shown in (b). Refined models with optimized parameters are shown in the inset taking into account 12, 13 and 14 atomic columns, where the most probable parametric model is the one containing 13 atomic columns as indicated by the MAP probability rule. (d) Synthetic ADF image of graphene obtained from an experimental 4D STEM dataset with an incoming electron dose of around $3 \cdot 10^5 e^-/Å^2$ and a minimum column CNR of around 6.1. (e) MAP probability rule evaluated for the experimental data shown in (d). (f) Most probable parametric model of the experimental data in (d) as indicated by the MAP probability rule in (e).

sense that it maximizes the probability of correctly detecting the model-order [31, 32]. In our case, the MAP probability rule can be written as

$$\mathrm{p}(\mathrm{N}|\mathbf{w}) = \frac{\mathrm{p}(\mathbf{w}|\mathrm{N})\mathrm{p}(\mathrm{N})}{\mathrm{p}(\mathbf{w})}, \tag{1}$$

where $\mathrm{p}(\mathrm{N}|\mathbf{w})$ denotes the posterior probability of the presence of N atomic columns in the image given the observed image pixel values $\mathbf{w}$. The MAP probability rule will select the number N that maximizes $\mathrm{p}(\mathrm{N}|\mathbf{w})$. The term $\mathrm{p}(\mathbf{w}|\mathrm{N})$ reflects the probability that the image data is generated by N atomic columns. The probability $\mathrm{p}(\mathrm{N})$ expresses prior knowledge of the number of atomic columns present in the image. Assuming there is no a priori preference for any number of columns, $\mathrm{p}(\mathrm{N})$ can be described as a uniform distribution. The denominator gives the probability of the image data irrespective of the knowledge about N. Since the denominator does not depend on N, it is omitted when comparing posterior probabilities with different N. Approximate analytical expressions for the MAP probability rule have been derived in the domains of molecular spectroscopy [33–35] and X-ray photoelectron spectroscopy (XPS) [36] by using calculation rules from probability theory. The same approach has been followed and an analogous analytical expression can be derived for ADF STEM when approximating the Poisson distribution, describing the number of detected electrons falling onto the detector, by a normal distribution [37, 38]. This approximation will already hold for a low number of detected electron counts per pixel. For Gaussian functions, an approximate analytical expression for the MAP probability rule is given by

$$\mathrm{p}(\mathrm{N}|\mathbf{w}) \propto \frac{\mathrm{N}! \cdot (4\pi)^{2\mathrm{N}} \cdot \mathrm{e}^{-\chi^2_{\mathrm{min}}/2}}{[(\eta_{\mathrm{max}} - \eta_{\mathrm{min}})(\rho_{\mathrm{max}} - \rho_{\mathrm{min}})]^{\mathrm{N}}} \times \frac{[\det(\nabla\nabla\chi^2)]^{-1/2}}{[(\beta_{\mathrm{x_{max}}} - \beta_{\mathrm{x_{min}}})(\beta_{\mathrm{y_{max}}} - \beta_{\mathrm{y_{min}}})]^{\mathrm{N}}}, \tag{2}$$

in which χ^2_{min} is the minimum weighted sum-of-squared residuals misfit between the data and the parametric model and $\det(\nabla\nabla\chi^2)$ is the determinant of the Hessian

matrix evaluated at $\chi^2_{\min}$. In this derivation, the weights are chosen to be equal to the experimental image pixel values. The symbols ρ, η and (β_x,β_y) refer to the width, intensity and coordinates of the Gaussian functions, respectively. The subscripts *max* and *min* refer to a predefined maximum and minimum value for the corresponding parameter.

As a first example, the MAP probability rule is verified by analyzing an experimental high-angle annular dark-field (HAADF) STEM image of a material with known structure, $SrTiO_3$. Images have been recorded by using a probe corrected FEI Titan, operated at 300 kV. The HAADF regime has been selected by using a semiconvergence angle of 21.3 mrad and a detector collection range of 58-197 mrad. A high CNR image is used as reference and is shown in figure 1(a). From this image, the brighter Sr columns and darker Ti-O columns are easily recognizable. The inset indicates the locations of both types of columns. Figure 1(b) shows a noisier counterpart of the inset of figure 1(a) with a 100 times lower electron dose. The dose was varied by defocusing the monochromator. Figure 1(c) shows the evaluation of the MAP probability rule for the image pixel values shown in figure 1(b) for an increasing number of atomic columns. Since the width of an atom column is mainly determined by the finite source size and to a lesser extent by the atom type, [39], a parametric model described by a superposition of Gaussian functions with equal widths has been used. From figure 1(c), it follows that the presence of 13 atomic columns is most probable corresponding to the expected crystal structure in [100] direction. Moreover, the MAP probability rule also provides a quantitative statement of how much more probable a certain number of columns is as compared to another number. Indeed, from figure 1(c) it can be derived that the probability of the presence of 13 atomic columns is around 63 times larger than 12 columns and around 3 times larger than 14 columns. Figure 1(d) shows a synthetic ADF image of graphene obtained from an experimental 4D STEM dataset with an acceleration voltage of 80 kV, semiconvergence angle of 24.8 mrad and a detector collection range of 26-50 mrad. Figure 1(e) shows the evaluation of the MAP probability rule to detect the C atoms of graphene from the low contrast data in figure 1(d), using a parametric model described by a superposition of Gaussian functions with equal widths. The most probable parametric model is shown in figure 1(f) clearly resolving the hexagonal lattice of graphene. It should be noted that the MAP probability rule obtained the expected structure of $SrTiO_3$ and graphene from images with a minimum column CNR of only 5.2 and 6.1, respectively, for which an ordinary peak finding routine, which searches for local maxima in the image by choosing an arbitrary threshold [16], failed. By changing the threshold, one can obtain a better result, but this approach relies heavily on visual inspection which will lead to biased structure information. Moreover, the MAP probability rule has been applied without introducing any prior knowledge concerning the atomic structure or chemical composition of $SrTiO_3$ or graphene. Calculations were performed using a single workstation resulting in a computation time of approximately 1 hour for the analysis of the $SrTiO_3$ image and approximately 11 hours for the graphene image.

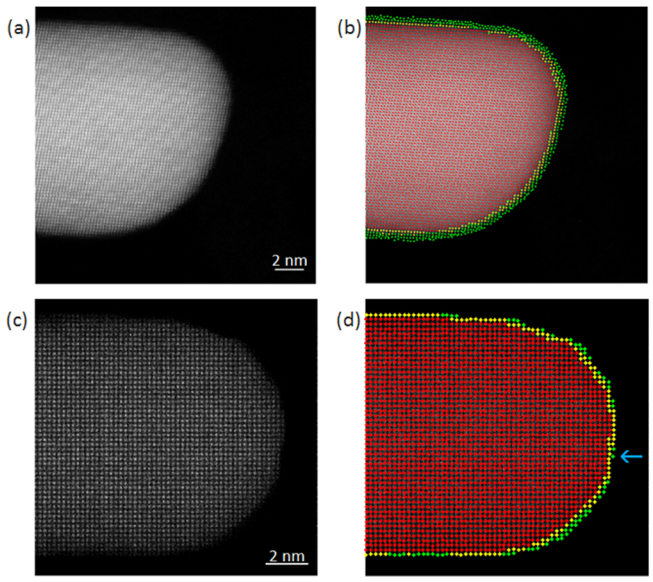

FIG. 2. (a) Experimental HAADF image of a Au nanorod with an incoming electron dose of around $2{\cdot}10^5$ $e^-/Å^2$ and a minimum column CNR of around 11.1. (b) Most probable atomic columns detected from (a) by a combination of an ordinary peak finding routine and the MAP probability rule near the edge of the rod, where columns in red have been detected by the ordinary peak finding routine, columns in yellow by both the ordinary peak finding routine and the MAP probability rule and columns in green by the MAP probability rule only. (c) Simulated HAADF image of a Au nanorod with the presence of Poisson noise with an incoming electron dose of 5000 $e^-/Å^2$ and a minimum column CNR of 8.9. (d) Most probable atomic columns detected from (c), where the arrow indicates an atom detected at a position where no atom was present.

As a next example, the method has been applied to an experimental and simulated HAADF STEM image of a Au nanorod, respectively. The experimental image is shown in figure 2(a) and was obtained by a double-aberration corrected FEI Titan operated at 300 kV and with a semiconvergence angle of 21.8 mrad and a detector collection range of 62-190 mrad [19]. It is noted that, due to the electron beam, especially surface atoms might not stay in the same position during the image acquisition [40]. The MAP probability rule has been used to identify the presence of atoms near the edge, which are difficult to detect visually. In this region

the rod is only a few atoms thick which, in combination with the relatively low incoming electron dose, leads to a low CNR. The following two-step procedure is suggested to determine the most probable structure of the Au nanorod. First, an ordinary peak finding routine is applied on the image. This routine is able to quickly detect most of the thicker columns, but has difficulties in correctly detecting atoms near the edge of the particle. Therefore, the MAP probability rule is applied to investigate the presence of atomic columns near the edge. The total intensity under a Gaussian function in the model has been chosen to be at least the total intensity scattered by a single Au atom, obtained from simulation with the MULTEM software [41, 42]. In this way, a specific value is assigned to $\eta_{\min}$ in expression (2). Furthermore, in order to take thickness fluctuations in the carbon support into account, the edge has been divided into different subregions. Their size has been selected such that the background in each subregion can adequately be modelled as a constant. This is the case when the size of a subregion is not larger than the maximum distance h_{max} upon which the variability of the background does not affect atom detection. The so-called variogram $\gamma(h)$ is a measure of the variability of the background as a function of distance h [43]. As a rule of thumb, the size of each subregion should obey $\Delta\gamma \leq \eta_{\min}^2/32$, which holds for the selected size of 10 Å by 10 Å. The result of the analysis is shown in figure 2(b). Columns in red have been found by the ordinary peak finding routine. Columns in yellow have been detected by both the ordinary peak finding routine and the MAP probability rule. Columns in green have been detected by the MAP probability rule only. It should be noted that at the edge there were no colums found by the ordinary peaking finding procedure which were not detected by the MAP probability rule. For radiation-sensitive materials, the incoming electron dose should be kept as low as possible. To illustrate the possibilities of the MAP probability rule when applied to low dose images, a 10 nm thick Au nanorod has been simulated using MULTEM with an acceleration voltage of 200 kV, a semiconvergence angle of 24 mrad, a detector collection range of 60-165 mrad and Gaussian source size broadening with a FWHM of 0.7 Å. In order to make the simulation more realistic, the structure has been fully relaxed by using molecular dynamics simulations employing the embedded atom method (EAM) potential [44] with the GPU Lammps package [45–47]. Figure 2(c) shows the simulated Au nanorod with an incoming electron dose of 5000 $e^-/Å^2$. For the analysis, the background has been put to zero since no carbon support is present in the simulation and the edge has been divided into 49 equal subregions to speed up the calculations. Figure 2(d) shows the detected atomic columns. From this analysis, it follows that all present atom columns have been detected and that only

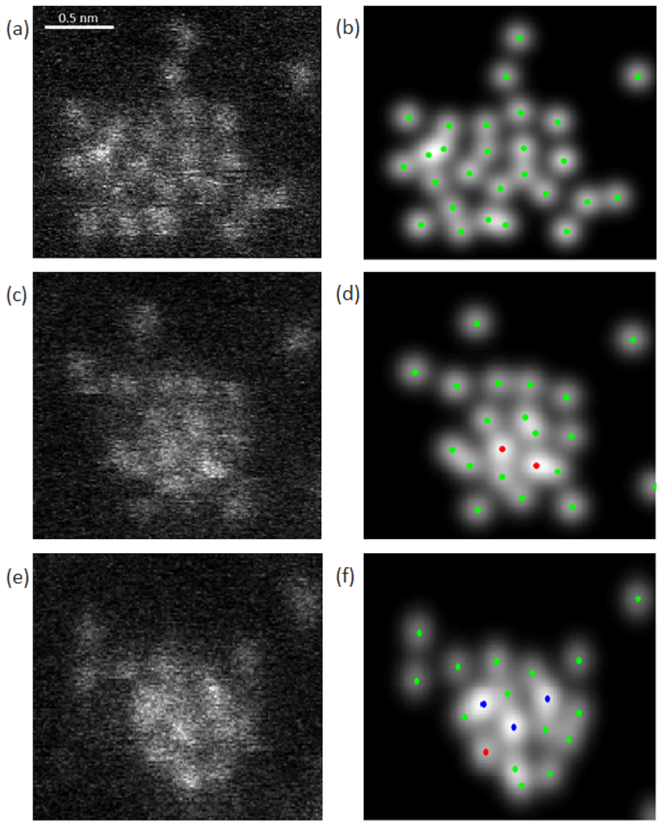

FIG. 3. (a),(c),(e) Sequence of HAADF STEM images of a Ge cluster with an incoming electron dose of around $6.8{\cdot}10^4$ $e^-/Å^2$ and a minimum column CNR of around 21.0. (b),(d),(e) Most probable parametric model of the experimental data in (a),(c),(e) indicated by the MAP probability rule with atom couting results added in which green, red and blue dots correspond to 1, 2 or 3 atoms, respectively.

one extra atom has been found at a position where the simulation did not include an atom. This atom is indicated by the blue arrow shown in figure 2(d). This probability for over- or underfitting is an inherent limitation of model-order selection methods and will in general increase with decreasing CNR. However, the present example demonstrates the excellent performance of the MAP probability rule when analyzing a low CNR image. Moreover, it can be seen from figures 2(b) and 2(d) that a substantial amount of atom columns would not have been detected in the absence of the MAP probability rule. This is an important result since it is well known that the exact surface morphology of nanoparticles can influence their physical properties.

The MAP probability rule is also of great importance to detect single atoms in ultrasmall nanoclusters. Such clusters can be thought of as fundamental building blocks leading to metamaterials with physical and chemical properties that are not available in nature [48, 49]. The growth mechanisms for small nanoclusters are much

more exotic than for bulk materials and therefore have a more complex structure. A series of HAADF STEM images of a small Ge cluster is shown in figures 3(a), 3(c) and 3(e). The clusters have been imaged using a double aberration-corrected FEI Titan operated at 120 kV and the beam current was set to 40 pA [50]. The MAP probability rule in combination with atom counting [51] can be used to verify whether there is no loss of atoms during the acquisition of the series of the images. In this analysis, one should, however, take into consideration that displacements of individual atoms are possible due to the interaction with the electron beam [40]. This may cause atoms to move in or out of the field of view. The MAP probability rule is used to determine the most probable structure of the cluster, using the intensity of a single Ge atom as prior knowledge, obtained from an image simulation with MULTEM. The most probable parametric models are shown in figures 3(b), 3(d) and 3(f), where the dots refer to estimated column positions. The volumes under the estimated Gaussian peaks are calculated to count the number of atoms in a column [51]. As compared to earlier results obtained by detecting atom columns by visual inspection of the images [50], the MAP probability rule detects more peaks, whereas the total number of atoms in each of the individual frames remains almost constant. The extra peaks correspond to atoms which are not perfectly aligned along the beam direction. This suggests that the MAP probability rule is able to disentangle strongly overlapping peaks resulting into more accurate structure information as compared to visual inspection. This is of great importance to fully understand the dynamics of such a small nanocluster.

In conclusion, the MAP probability rule has been introduced to detect single atoms from low CNR STEM images. By combining parameter estimation and model-order selection, the most probable atomic structure of unknown nanomaterials can be determined in an automatic and objective manner. This information is of great importance for the analysis of radiation-sensitive and light-element nanostructures, where a visual inspection of images may lead to biased results. In addition, the MAP probability rule enables one to quantify how more likely the result is as compared to other atomic structures. The validity and usefulness of the MAP probability rule has been demonstrated to experimental and simulated ADF STEM images of samples of arbitrary shape, size, and atom type. The MAP probability rule has been implemented in the freely available StatSTEM software [16].

The authors acknowledge financial support from the Research Foundation Flanders (FWO, Belgium) through Project No. G.0368.15N. The authors are grateful to M. Van Bael and P. Lievens (KU Leuven) and to L. M. Liz-Marzán (CIC biomaGUNE and Ikerbasque) for providing the samples. This project has received funding from the European Research Council (ERC) under the European Unions Horizon 2020 research and innovation programme (grant agreement No 770887).

* Sandra.VanAert@uantwerpen.be

[1] O. L. Krivanek, N. Dellby, and M. F. Murfitt, in *Handbook of Charged Particle Optics* (CRC Press, Boca Raton, Florida, 2009), pp. 601-641.
[2] H. H. Rose, J. Elect. Microsc. **58**, 77-85 (2009).
[3] P. W. Hawkes, Ultramicroscopy **156**, A1-64 (2015).
[4] J. E. Allen, E. R. Hemesath, D. E. Perea, J. L. Lensch-Falk, Z. Y. Li, F. Yin, M. H. Gass, P. Wang, A. L. Bleloch, R. E. Palmer, and L. J. Lauhon, Nat. Nanotech. **3**, 168-173 (2008).
[5] K. Urban, Science **321**, 506-510 (2008).
[6] C. L. Jia, S. B. Mi, M. Faley, U. Poppe, J. Schubert, and K. Urban, Phys. Rev. B **79**, 081405 (2009).
[7] R. Erni, M. D. Rossell, C. Kisielowski, and U. Dahmen, Phys. Rev. Lett. **102**, 096101 (2009).
[8] H. Sawada, Y. Tanishiro, N. Ohashi, T. Tomita, F. Hosokawa, T. Kaneyama, Y. Kondo, and K. Takayanagi, J. Electr. Micr. **58**, 357-361 (2009).
[9] O. L. Krivanek, M. F. Chisholm, V. Nicolosi, T. J. Pennycook, G. J. Corbin, N. Dellby, M. F. Murfitt, C. S. Own, Z. S. Szilagyi, M. P. Oxley, S. T. Pantelides, and S. J. Pennycook, Nature **464**, 571-574 (2010).
[10] V. Oltalan, A. Uzun, B. C. Gates, and N. D. Browning, Nat. Nanotech. **5**, 843-847 (2010).
[11] J. Hwang, J. Y. Zhang, A. J. D'Alfonso, L. J. Allen, and S. Stemmer, Physi. Rev. Lett. **111**, 266101 (2013).
[12] R. Ishikawa, R. Mishra, A. R. Lupini, S. D. Findlay, T. Taniguchi, S. T. Pantelides, and S. J. Pennycook, Phys. Rev. Lett. **113**, 155501 (2014).
[13] A. J. den Dekker, S. Van Aert, A. van den Bos, and D. Van Dyck, Ultramicroscopy **104**, 83-106 (2005).
[14] S. Van Aert, A. J. den Dekker, A. van den Bos, D. Van Dyck, and J. H. Chen, Ultramicroscopy **104**, 107-125 (2005).
[15] A. J. den Dekker, J. Gonnissen, A. De Backer, J. Sijbers, and S. Van Aert, Ultramicroscopy **134**, 34-43 (2013).
[16] A. De Backer, K. H. W. van den Bos, W. Van den Broek, J. Sijbers, and S. Van Aert Ultramicroscopy **171**, 104-116 (2016).
[17] S. D. Findlay, Y. Kohno, L. A. Cardamone, Y. Ikuhara, and N. Shibata, Ultramicroscopy **136**, 31-41 (2014).
[18] S. Van Aert, J. Verbeeck, R. Erni, S. Bals, M. Luysberg, D. Van Dyck, and G. Van Tendeloo, Ultramicroscopy **109**, 1236-1244 (2009).
[19] S. Van Aert, A. De Backer, G. T. Martinez, B. Goris, S. Bals, G. Van Tendeloo, and A. Rosenauer, Phys. Rev. B **87**, 064107 (2013).
[20] H. E, K. E. MacArthur, T. J. Pennycook, E. Okunishi, A. J. D'Alfonso, N. R. Lugg, L. J. Allen, and P. D. Nellist, Ultramicroscopy **133**, 109-119 (2013).
[21] S. Van Aert, K. J. Batenburg, M. D. Rossell, R. Erni, and G. Van Tendeloo, Nature, **470**, 374-377 (2011).
[22] S. Bals, M. Casalova, M. A. van Huis, S. Van Aert, K. J. Batenburg, G. Van Tendeloo, and D. Vanmaekelbergh, Nano Lett. **11**, 3420-3424 (2011).

[23] S. Van Aert, S. Turner, R. Delville, D. Schryvers, G. Van Tendeloo, and E. K. Salje Adv. Mat. **24**, 523-527 (2012).

[24] G. T. Martinez, A. Rosenauer, A. De Backer, J. Verbeeck, and S. Van Aert, Ultramicroscopy **137**, 12-19 (2014).

[25] H. Akamine, K. H. W. van den Bos, N. Gauquelin, S. Farjami, S. Van Aert, D. Schryvers, and M. Nishida, J. Alloys and Compd. **644**, 570-574 (2015).

[26] K. H. W. van den Bos, A. De Backer, G. T. Martinez, N. Winckelmans, S. Bals, P. D. Nellist, and S. Van Aert, *Phys. Rev. Lett.* **116**, 246101 (2016).

[27] P. D. Nellist, and S. J. Pennycook J. Microsc. **190**, 159-170 (1998).

[28] J. C. Meyer, J. Kotakoski, C. Mangler Ultramicroscopy **145**, 13-21 (2014).

[29] E. T. Jaynes, in *Probability theory: The logic of science* (Cambridge University Press, Cambridge, 2003).

[30] D. S. Sivia, and J. Skilling, in *A Bayesian tutorial* (Oxford University Press, Oxford, 2006).

[31] H. L. Van Trees, in *Detection, Estimation, and Modulation Theory, Part I* (Wiley, New York, 1968).

[32] L. L. Scharf, in *Statistical Signal Processing - Detection, Estimation and Time Series Analysis* (Addison-Wesley, Reading, Massachusetts, 1991).

[33] D. S. Sivia, and C. J. Carlile, J. Chem. Phys. **96**, 170-178 (1992).

[34] D. S. Sivia, C. J. Carlile, W. S. Howells, Physica B **182**, 341-348 (1992).

[35] D. S. Sivia, W. I. F. David, and K. S. Knight, Physica D **66**, 234-242 (1993).

[36] N. Armstrong, and D. B. Hibbert, Chemometr. Intell. Lab. Syst. **97**, 194-210 (2009).

[37] A. Papoulis, in *Probability, Random Variables, and Stochastic Processes* (McGraw-Hill, New York, 1965).

[38] K.-H. Herrmann, in *Image Recording in Microscopy. Handbook of Microscopy - Applications in Materials Science, Solid State Physics and Chemistry* (VCH, Weinheim, 1997).

[39] J. M. LeBeau, and S. Stemmer, Ultramicroscopy **108**, 1653-1658 (2008).

[40] D. B. Williams and C. B. Carter, in *Transmission Electron Microscopy* (Plenum Press, New York, 1996).

[41] I. Lobato, and D. Van Dyck, Ultramicroscopy **156**, 9-17 (2015).

[42] I. Lobato, S. Van Aert, and J. Verbeeck, Ultramicroscopy **168**, 17-27 (2016).

[43] G. Matheron, Econ. Geol., **58**, 1246-1266 (1963).

[44] S. M. Foiles, M. I. Baskes, and M. S. Daw, Phys. Rev. B **33**, 7983-7991 (1986).

[45] W. M. Brown, P. Wang, S. J. Plimpton, and A. N. Tharrington, Comput. Phys. Commun. **182**, 898-911 (2011).

[46] W. M. Brown, A. Kohlmeyer, S. J. Plimpton, and A. N. Tharrington, Comput. Phys. Commun. **183**, 449-459 (2012).

[47] W. M. Brown, and M. Yamada, Comput. Phys. Commun. **184**, 2785-2793 (2013).

[48] C. Binns, Surf. Sci. Rep. **44**, 1-49 (2001).

[49] S. A. Claridge, A. W. Castleman, S. N. Khanna, C. B. Murray, A. Sen, and P. S. Weiss, ACS Nano **3**, 244-255 (2009).

[50] S. Bals, S. Van Aert, C. P. Romero, M. J. Lauwaet, B. Schoeters, B. Partoens, E. Yucelen, P. Lievens, and G. Van Tendeloo, Nat. Comm. **3**, 897 (2012).

[51] A. De Backer, G. T. Martinez, A. Rosenauer, and S. Van Aert, Ultramicroscopy **134**, 23-33 (2013).